NANO LETTERS

pubs.acs.org/NanoLett Letter

Probing Hybrid $LiFePO_4/FePO_4$ Phases in a Single Olive $LiFePO_4$ Particle and Their Recovering from Degraded Electric Vehicle Batteries

Wenyu Wang, Rui Wang, Renming Zhan, Junmou Du, Zihe Chen, Ruikang Feng, Yuchen Tan, Yang Hu, Yangtao Ou, Yifei Yuan, Cheng Li, Yinguo Xiao, and Yongming Sun*

Cite This: https://doi.org/10.1021/acs.nanolett.3c01991 Read Online

ACCESS | Metrics & More | Article Recommendations | Supporting Information

ABSTRACT: The recycling of $LiFePO_4$ from degraded lithium-ion batteries (LIBs) from electric vehicles (EVs) has gained significant attention due to resource, environment, and cost considerations. Through neutron diffraction, X-ray photoelectron spectroscopy, and transmission electron microscopy, we revealed continuous lithium loss during battery cycling, resulting in a Li-deficient state ($Li_{1-x}FePO_4$) and phase separation within individual particles, where olive-shaped $FePO_4$ nanodomains (5−10 nm) were embedded in the $LiFePO_4$ matrix. The preservation of the olive-shaped skeleton during Li loss and phase change enabled materials recovery. By chemical compensation for the lithium loss, we successfully restored the hybrid $LiFePO_4/FePO_4$ structure to pure $LiFePO_4$, eliminating nanograin boundaries. The regenerated $LiFePO_4$ (R-$LiFePO_4$) exhibited a high crystallinity similar to the fresh counterpart. This study highlights the importance of topotactic chemical reactions in structural repair and offers insights into the potential of targeted Li compensation for energy-efficient recycling of battery electrode materials with polyanion-type skeletons.

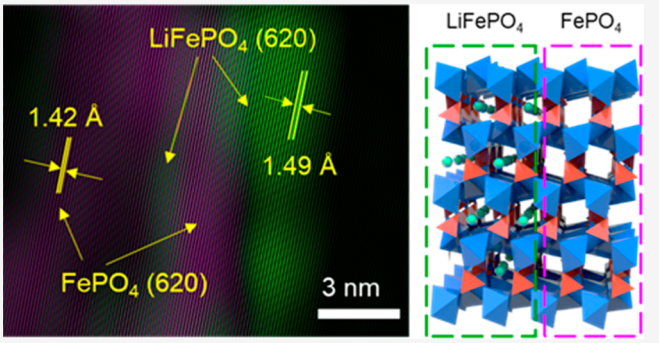

KEYWORDS: *hybrid $LiFePO_4/FePO_4$, single particle, targeted Li compensation, regeneration, degraded lithium-ion batteries*

With an overwhelming demand of 550 GWh in 2022, lithium-ion batteries (LIBs) have long-term been the main power sources for electric vehicles (EVs) and consumer electronics.[1] The postprocessing of the consequent millions of tons of degraded LIBs is becoming a crucial challenge after their service.[2] Therefore, a call arises for an effective approach for low-cost, energy-saving recycling of key electrode materials (mainly cathode materials, such as $LiFePO_4$, $LiCoO_2$, and $LiNi_{1-x-y}Co_xMn_yO_2$) containing valuable metal elements, which can mitigate the issue of environmental pollution and enable high utilization of resources.[3,4] Currently, the main recycling approaches for spent cathode materials include hydrometallurgy and pyrometallurgy.[5,6] They involve the transition of degraded active materials to initial raw materials and materials resynthesis.[7] Using the recycling of $LiFePO_4$ as a typical example, degraded $LiFePO_4$ is often treated with acids (H_3PO_4, HCl, H_2SO_4, etc.) for lithium extraction,[8] which produces lithium compounds (Li_2CO_3, LiOH, etc.) and iron compounds ($FePO_4$, $FeSO_4$, etc.). Coprecipitation coupled with heat treatment procedures is further conducted for the regeneration of $LiFePO_4$ using the above obtained intermediates.[9] However, such an approach often brings issues of high energy consumption, high cost, abundant greenhouse gas emissions, and high consumption of acid and alkali chemicals.[10−13] Recently, direct regeneration of $LiFePO_4$ has been proposed,[14−18] which avoids the multiple-step operations with complex equipment and the use of plenty of acid/alkali chemicals. Besides, several studies take the direction of new applications for degraded cathodes, such as lithium extraction from salt lakes[19] and cathode materials for dual-ion batteries.[20] For direct recycling/regeneration, analysis of the physicochemical state of active materials should be first conducted, including the composition and phase structure, to determine the possibility of direct regeneration, which remains a significant challenge until now.[21] With precise materials characterizations, one can judge the feasibility of regeneration of degraded active materials by employing facile chemical or low-temperature thermal treatments with low energy consumption and low cost.[22]

Received: May 28, 2023
Revised: July 17, 2023

In this work, using lithium-ion phosphate ($LiFePO_4$) as a model system, we evaluated the feasibility of direct material repair based on precise phase structure and component analysis and investigated the structure evolution during its recovering. After long-term cycling, part of the olivine $LiFePO_4$ converted to $FePO_4$, leading to the overall materials composition of $Li_{1-x}FePO_4$. We revealed the coexistence of $LiFePO_4$ and $FePO_4$ within one single D-$LiFePO_4$ particle, where the $FePO_4$ domains were randomly distributed in the particle. It is noted that both $LiFePO_4$ and $FePO_4$ possessed high crystallinity of the olivine structure with only slight lattice variations, providing the basis for direct materials repairing. Experimentally, the phase transition and structure recovering were monitored by high resolution transmission electron microscopy (HRTEM) and neutron diffraction after chemical Li filling. The successful conversion from $FePO_4$ to $LiFePO_4$ eliminated the phase separation in one single particle, and the recovered $LiFePO_4$ showed electrochemical performance comparable to that of the fresh counterpart (Figure 1). The

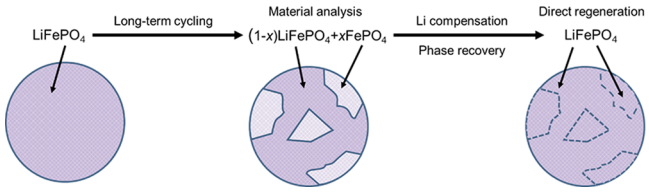

Figure 1. Schematic illustration of the targeted lithium compensation process.

use of a Li-arene solution provides a facile approach for Li refilling in degraded $LiFePO_4$ compared to the other strategies, including hydrometallurgy, pyrometallurgy, and hydrothermal methods. It avoids complex and time-consuming procedures, and reduces the energy consumption. Besides, the used reagent can be effectively recycled via its reaction with metallic Li, demonstrating the potential low cost for this approach.

D-$LiFePO_4$ was obtained from a retired electric vehicle battery (a 30Ah laminated $LiFePO_4$||graphite pouch cell at the discharge state, Figure 2a). Before its retirement, it kept working for over 3000 charge/discharge cycles on an electric bus with a serving time of over eight years. After cell disassembly, the D-$LiFePO_4$ cathode was separated from other battery components (e.g., the graphite anode and separator). It was found that the D-$LiFePO_4$ cathode remained as an integrated structure with a plat and smooth surface without obvious scratches/cracks or exfoliation from the current collector. X-ray diffraction (XRD) was employed to investigate the crystallinity and phase information on the D-$LiFePO_4$ cathode (Figure S1). The prominent XRD diffraction peaks of D-$LiFePO_4$ can be readily indexed to orthorhombic olivine $LiFePO_4$ (space group: *Pnma*, JCPDS No. 83-2092). Besides, four weak peaks at 18.2°, 30.4°, 31.0°, and 37.5° were shown, which could be ascribed to the $FePO_4$ phase (space group: *Pnma*, JCPDS No. 42-0579).[16,23,24] For an ideal $LiFePO_4$|| graphite cell at the discharge state, all the active Li fills in the crystal structure of the cathode, forming a pure olivine $LiFePO_4$ phase without Li vacancy. During repeated charge/discharge cycling, continuous active Li loss occurs, leading to Li deficiency at the cathode and causing the formation of mixed phases of $LiFePO_4$ and $FePO_4$.[25,26] The D-$LiFePO_4$ and fresh $LiFePO_4$ (F-$LiFePO_4$) from the same materials company were further subjected to neutron diffraction for collecting more detailed structural information. Figure 2b and Figure S2 compare the neutron diffraction patterns and Rietveld refinement curves of F-$LiFePO_4$ and D-$LiFePO_4$. Based on the results of Rietveld refinement, the lattice parameters of F-$LiFePO_4$ were 10.3329(2) Å, 6.0094(2) Å, and 4.6922(2) Å for *a*, *b*, and *c*, respectively. As shown in Figure 2c and Table S1, $LiFePO_4$ has an orthorhombic lattice structure in a space group *Pnma*, where P^{5+} is located in the 4*c* tetrahedral site, and Li^+ and Fe^{2+} occupy the 4*a* and 4*c* octahedral sites, respectively.[27] In the *b*−*c* plane, FeO_6 shares corners in the shape of a zigzag line, and LiO_6 is edge-shared in parallel chains that allow Li^+ diffuse fast along the [010] direction.[28−31] The results of neutron diffraction patterns and Rietveld refinement revealed that D-$LiFeO_4$ possessed mixed phases of $FePO_4$ and $LiFePO_4$ and their proportions were 60.8% and 39.2%, respectively. Different from $LiFePO_4$, the Li in 4*a* octahedral sites in the olivine structure is absent for $FePO_4$, leaving full vacancies at this site. The Li−Fe antisite concentrations in F-$LiFePO_4$ and D-$LiFePO_4$ were compared according to the neutron diffraction results (inset in Figures 2b and S2; Tables S1 and S2). The Li−Fe antisite concentration of D-$LiFePO_4$ increased significantly compared to that of the F-$LiFePO_4$ (1.4% for F-$LiFePO_4$, 3.7% for D-$LiFePO_4$), suggesting structural degradation of $LiFePO_4$ on cycling. The charge Li-ion specific capacity of the mixed phases was then calculated as 58.8 mAh g^{-1} according to the proportions of $FePO_4$ and $LiFePO_4$ phases. Experimentally, D-$LiFePO_4$ was electrochemically charged for delithiation, and the initial Li-ion charge capacity was 54.4 mAh g^{-1} (Figure S3), in good agreement with the above analysis. Note that in the Li metal half cell configuration, the specific capacity of D-$LiFePO_4$ after the initial cycle can be increased to the level of F-$LiFePO_4$ (150.4 mAh g^{-1}, Figure S3), indicating the good stability of the cycled olive structured framework and potential of materials recovering for D-$LiFePO_4$ through a simple electrochemical/chemical processing with Li filling. High-resolution X-ray photoelectron spectroscopy (XPS) spectra of Fe 2p were provided for F-$LiFePO_4$ and D-$LiFePO_4$ (Figure 2e). The peaks for Fe^{2+} at 710.5 eV ($2p_{3/2}$) and 724 eV ($2p_{1/2}$) were prominent for the F-$LiFePO_4$, while peaks for Fe^{3+} at 712.5 eV ($2p_{3/2}$) and 725.5 eV ($2p_{1/2}$) were dominating for D-$LiFePO_4$,[32] which also supported the generation of $FePO_4$ phase in the D-$LiFePO_4$ electrode. The weak Fe^{3+} peaks in the high-resolution Fe 2p spectra in Figures 2e and 3c could be ascribed to its slight surface oxidation.[33−35]

The morphology of D-$LiFePO_4$ was investigated by scanning electron microscopy (SEM). Monodispersed particles with sizes <200 nm and aggregates with sizes <500 nm were both observed. No cracks were shown for all of the particles in the measured area, indicating the overall good structural stability of D-$LiFePO_4$ (Figure S4a). It should be noted that good integrity of the degraded active materials plays an important role in their direct regeneration.[20] Usually, cracks or scratches cannot be recovered unless high-temperature annealing for recrystallization is employed. The structural information was further revealed by HRTEM. Figure 2f shows the lattice fringe of a D-$LiFePO_4$ particle, and the corresponding spotty fast Fourier transform (FFT) pattern is shown in Figure 2h, which could be well indexed to the (310) and (011) crystal planes along the [1-33] zone axis. It was noted that the (620) reflection spot was split into two spots corresponding to *d*-spacing of 1.52 and 1.43 Å, respectively (calculated $LiFePO_4$ d_{620} = 1.49 Å, calculated $FePO_4$ d_{620} = 1.42 Å). Thus, the

https://doi.org/10.1021/acs.nanolett.3c01991
Nano Lett. XXXX, XXX, XXX−XXX

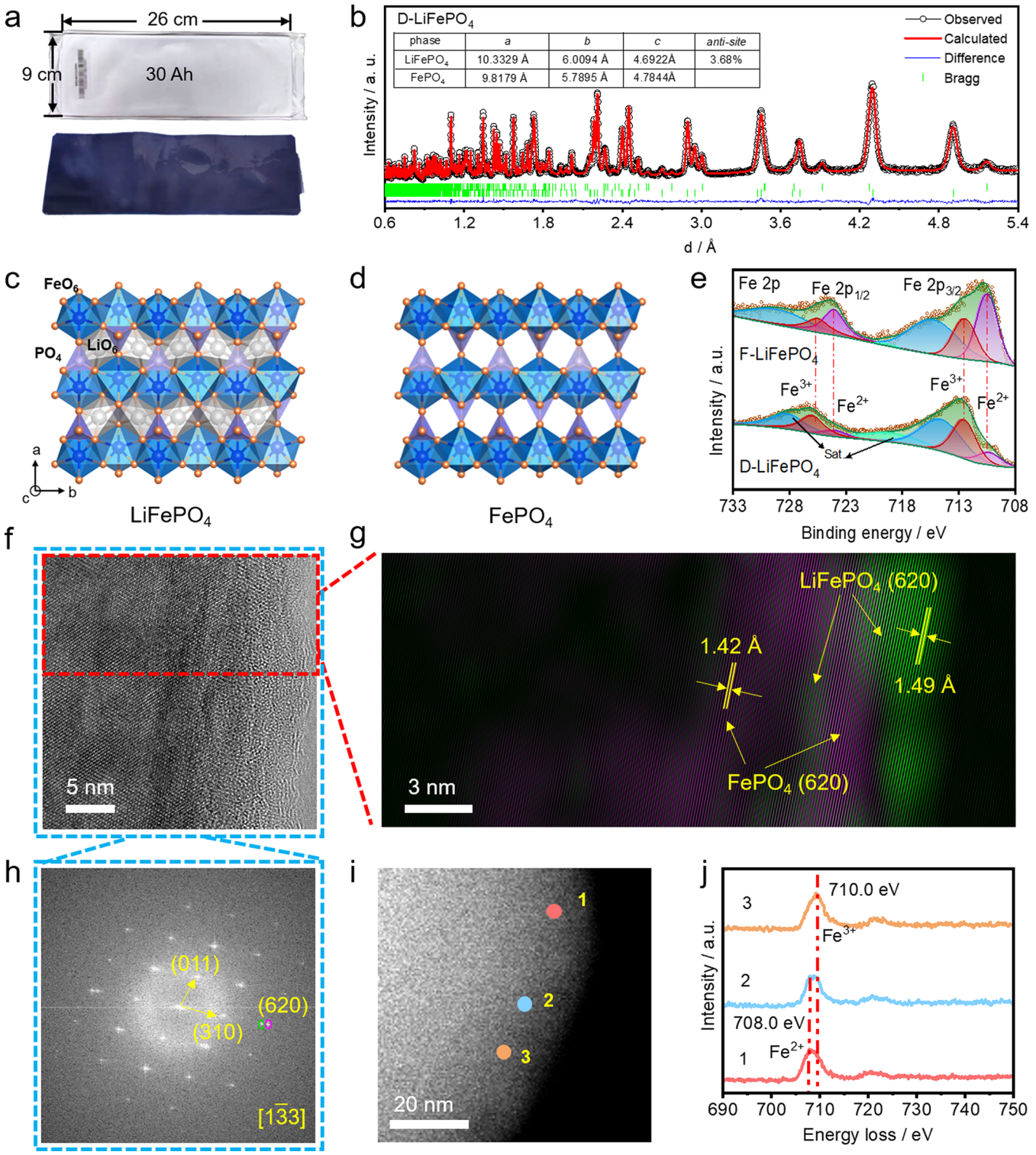

Figure 2. (a) Photograph of a 30 Ah D-LiFePO$_4$||graphite cell. (b) Neutron diffraction Rietveld refinement result of D-LiFePO$_4$. Crystal structure of (c) LiFePO$_4$ and (d) FePO$_4$. (e) High-resolution Fe 2p XPS spectrum of D-LiFePO$_4$ and F-LiFePO$_4$. (f) HRTEM image of D-LiFeO$_4$. (g) (620) lattice distribution of LiFePO$_4$ (green) and FePO$_4$ (red) in a D-LiFePO$_4$ particle based on the Fourier transform of the HRTEM image. (h) Fast Fourier transform from D-LiFePO$_4$ in panel f showing (310) and (011) lattice reflections. (i) STEM image and (j) Fe L-edge EELS spectra of D-LiFePO$_4$.

coexistence of FePO$_4$ and LiFePO$_4$ phases was verified, which suggested the transformation of LiFePO$_4$ to FePO$_4$ during the long-term cycling of batteries. The distribution of FePO$_4$ and LiFePO$_4$ could be obtained by the inverse FFT of the (620) reflection spot (Figure 2g). High-angle annular dark-field scanning TEM (HAFDF-STEM) and electron energy loss spectroscopy (EELS) measurements were further employed to investigate the microstructure and composition of D-LiFePO$_4$. HAADF-STEM images in Figures 2i and S5 revealed the uniform and intact microstructure of a D-LiFePO$_4$ particle,

https://doi.org/10.1021/acs.nanolett.3c01991
Nano Lett. XXXX, XXX, XXX−XXX

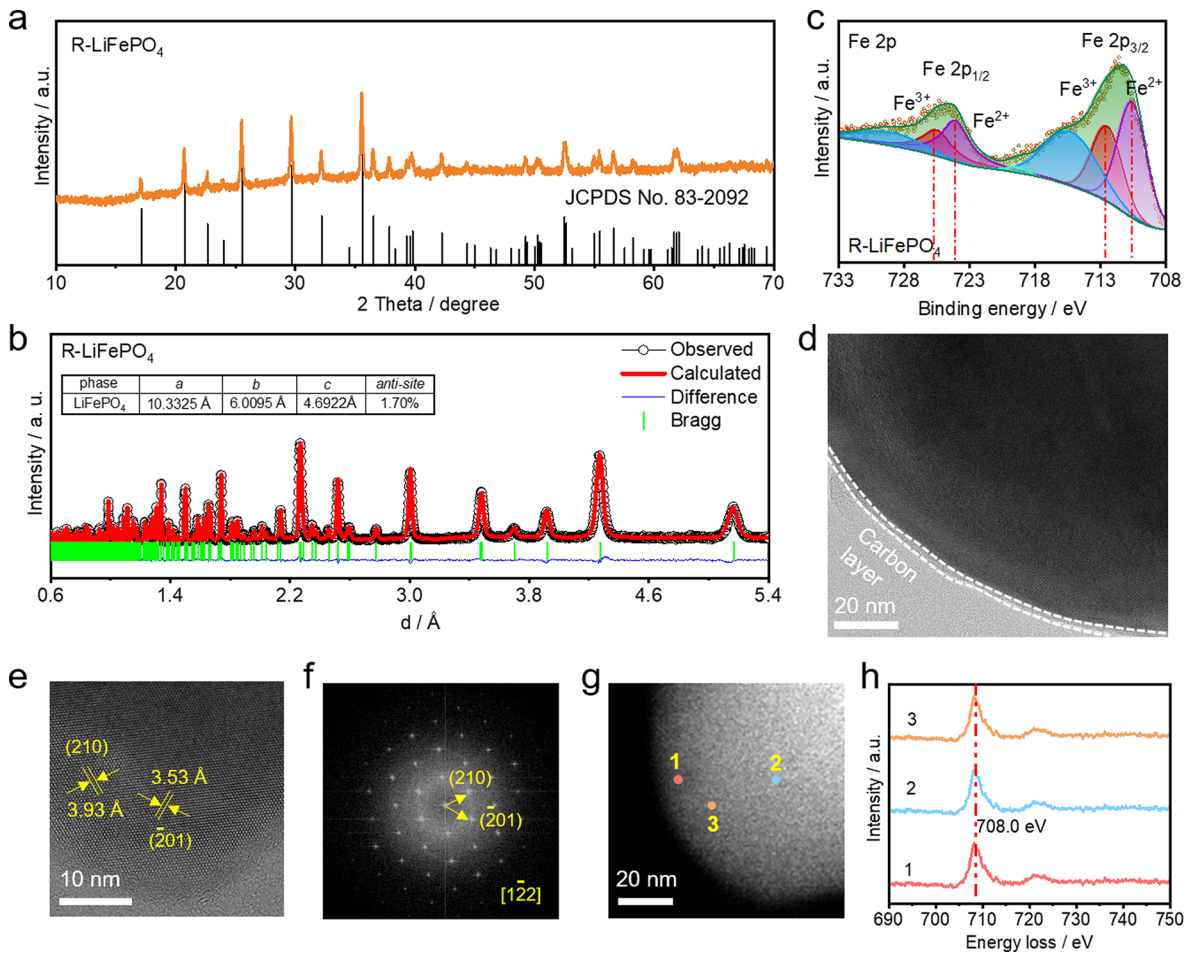

Figure 3. (a) XRD patterns and (b) neutron diffraction Rietveld refinement results and (c) high-resolution Fe 2p XPS spectrum of R-$LiFePO_4$ (d) TEM and (e) HRTEM of R-$LiFePO_4$. (f) Fast Fourier transform of Figure 3e showing (210) and (−201) lattice reflection. (g) STEM image and (h) Fe L-edge EELS spectra of R-$LiFePO_4$.

further verifying the excellent structural integrity of D-$LiFePO_4$ after cycling. Fe L-edge EELS spectra collected in the labeled locations (located at 1−3) of one D-$LiFePO_4$ particle (Figure 2i) are provided in Figure 2j. At location 1, the Fe L-edge showed a dominant peak at ∼708.0 eV, which could be ascribed to Fe^{2+}. At location 2, there existed a peak at ∼710 eV for Fe^{3+} besides the peak at ∼708 eV, suggesting the coexistence of Fe^{3+} and Fe^{2+}.[36] The peak for Fe^{3+} was shown only at location 3. All of the above results again supported the transformation of $LiFePO_4$ to $FePO_4$ due to the active Li loss as well as structural degradation after long-term battery cycling. Thus, one main degradation mechanism for D-$LiFePO_4$ from electric vehicles is Li loss and the transition of Fe^{2+} to Fe^{3+}, which cause the generation of the $FePO_4$ phase embedded in $LiFePO_4$. Such a mechanism provides opportunities for facile materials regeneration by targeted Li refilling in 4a sites of olive structured $FePO_4$. Also, the intact particle structure of D-$LiFePO_4$ makes for the potential of using mild materials processing for recovery.

Olivine phosphate polyanionic materials possessed a robust crystal structure, which remained stable even under harsh materials processing. We conducted a Li-arene solution ($C_{10}H_8Li$) treatment operation for targeted Li filling and Fe^{3+} reduction of D-$LiFePO_4$.[37,38] Figure 3a shows the XRD result of R-$LiFePO_4$. The peaks for $FePO_4$ in D-$LiFePO_4$ disappeared, and all of the diffraction peaks could be ascribed to the olive $LiFePO_4$ phase, suggesting the successful phase recovery and Li filling after mild solution processing. Neutron diffraction and Rietveld refinement were further conducted to verify the recovery of components and structures of D-$LiFePO_4$ (Figure 3b and Table S3). No $FePO_4$ phase was observed in R-$LiFePO_4$. The lattice parameters of R-$LiFePO_4$ were 10.3325(2) Å, 6.0095(2) Å, and 4.6922(2) Å for *a*, *b*, and *c*, which were very close to those of F-$LiFePO_4$ before cycling. Only a slight amount of Li/Fe antisite of 1.7% existed in R-$LiFePO_4$, indicating the successfully targeted Li filling into the 4a site of olivine $LiFePO_4$. The surface chemical state of R-$LiFePO_4$ was measured by XPS. A high-resolution Fe 2p XPS spectrum showed dominative peaks of Fe^{2+} at 710.5 eV ($2p_{3/2}$) and 724 eV($2p_{1/2}$), in sharp contrast to much weaker ones in D-$LiFePO_4$, again supporting the transition of Fe^{3+} to Fe^{2+} during the solution reaction of chemical Li filling (Figure 3c).[32]

The morphology of R-$LiFePO_4$ was further investigated. After targeted Li compensation and structure recovery, all of the particles in the measured area under SEM maintained an intact structure without any cracks (Figure S4b). Also, the result of TEM indicated that the original carbon coating layer with a thickness of ∼2 nm was well remained on the surface of the R-$LiFePO_4$ particle, as well as the intact particle structure, showing the significant advantage of using a solution-based repairing approach in maintaining the structure/morphology

https://doi.org/10.1021/acs.nanolett.3c01991
Nano Lett. XXXX, XXX, XXX−XXX

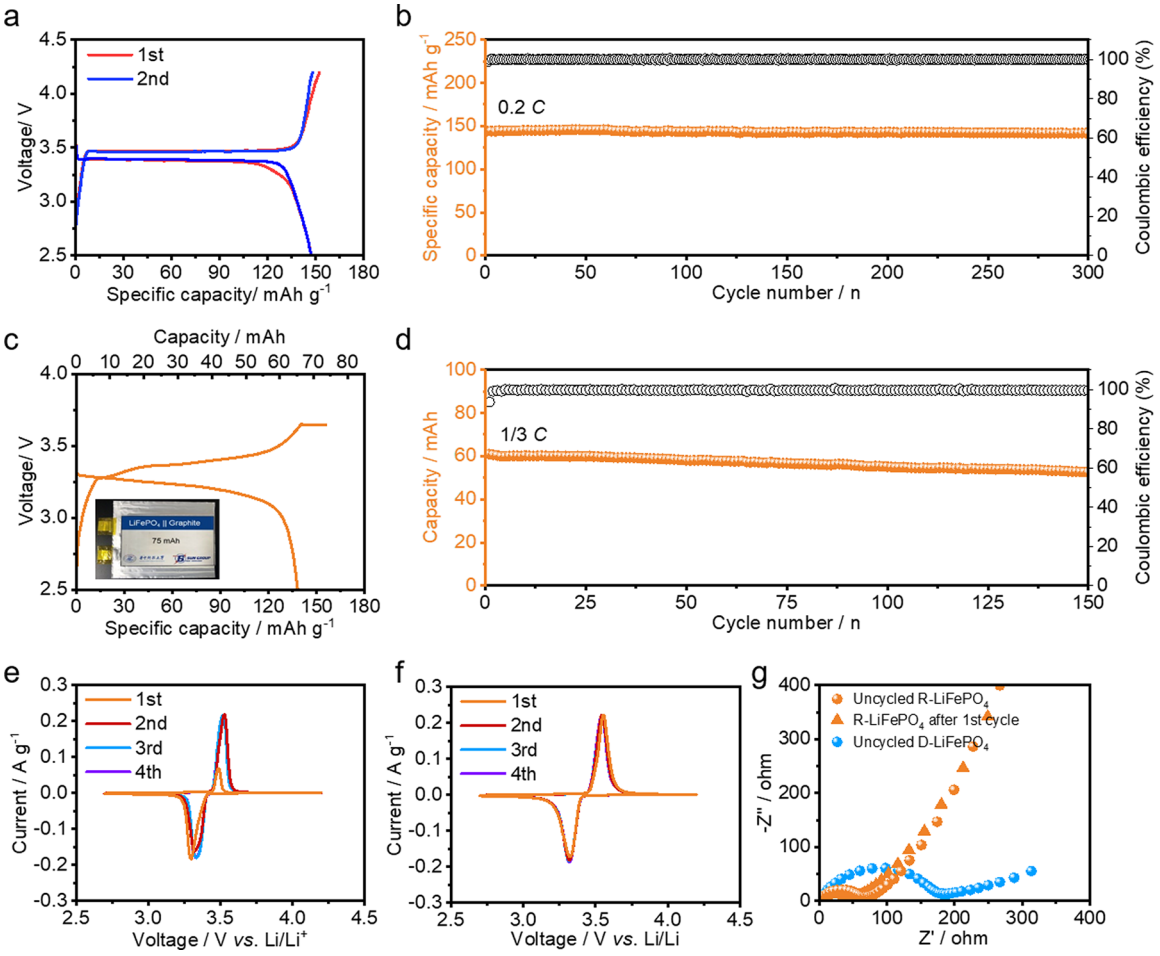

Figure 4. (a) Charge−discharge curves of R-$LiFePO_4$ in half-cell configurations for the first and second cycles. (b) Capacity-cycle number and CE-cycle number plots of R-$LiFePO_4$ at 0.2 C in a half-cell configuration. (c) Initial charge−discharge curves of R-$LiFePO_4$ and (d) capacity-cycle number plot of R-$LiFePO_4$||graphite pouch cell at 1/3 C. CV profiles for (e) D-$LiFePO_4$ and (f) R-$LiFePO_4$ at 0.1 mV s^{-1}. (g) Nyquist plots of the uncycled D-$LiFePO_4$ (blue) and uncycled R-$LiFePO_4$ (orange, cycle) and R-$LiFePO_4$ (orange, triangle) electrodes after the first cycle in the frequency range of 100 mHz−1000 kHz.

integrity (Figure 3d). Thus, no further carbon coating or approach is required for realizing the high electrochemical performance of R-$LiFePO_4$. The HRTEM image showed continuous lattice fringes over the entire measured area (Figure 3e) and its Fast Fourier transform pattern could be well indexed as the (210) and (−201) crystal planes for $LiFePO_4$ along the [1-22] zone axis (Figure 3f) with the spacing distances of 3.94 and 3.58 Å, respectively. In comparison to the result of D-$LiFePO_4$, no spot splitting occurred for R-$LiFePO_4$, which revealed the complete conversion of the $FePO_4$ phase to the $LiFePO_4$ phase. The same results were also observed for 4 other active particles, suggesting high consistency (Figure S6). The above results again support the successful regeneration of D-$LiFePO_4$.

The microstructure and composition of R-$LiFePO_4$ were further investigated by high-angle annular dark-field scanning TEM (HAFDF-STEM) and EELS measurement. HAADF-STEM images in Figures 3g and S7 revealed that the R-$LiFePO_4$ particles maintained a uniform and intact microstructure after materials processing. Figure 3h shows EELS spectra of Fe L-edge collected in different locations (locations 1−3) of one R-$LiFePO_4$ particle (Figure 3g). Different from the coexistence of the Fe L-edge for Fe^{2+} and Fe^{3+} for D-$LiFePO_4$, only the Fe L-edge at ∼708.0 eV for Fe^{2+} was observed for the measured three different locations for R-$LiFePO_4$. All the above results again verify the successful composition recovery after targeted Li compensation. Two key parameters for D-$LiFePO_4$ recovery with a high level of quality are concluded as follows: 1) Targeted Li compensation into 4a site in olivine $FePO_4$ and the reduction of Fe^{3+} to Fe^{2+}.[33] 2) The good structural stability of $LiFePO_4$ during the processing. With respect to the above two aspects, the as-employed solution based chemical targeted Li compensation approach is successful in D-$LiFePO_4$ regeneration.

The electrochemical performances of R-$LiFePO_4$ were first investigated in half cells. The R-$LiFePO_4$ delivered a reasonable specific capacity of 152.5 mAh g^{-1} at 0.1 C in the voltage range between 2.5 and 4.2 V (close to that of F-$LiFePO_4$), suggesting the success of active Li filling (Figures 4a and S8). Figure 4b shows the capacity-cycle number plot of R-$LiFePO_4$. The electrode displayed a reversible specific capacity of 146.0 mAh g^{-1} at 0.2 C and showed a high capacity retention of 98.1% for 300 cycles. For full pouch cell measurement, a batch of ∼20 g of R-$LiFePO_4$ was fabricated (Figure S10) and $LiFePO_4$||graphite pouch cell was assembled (Figure 4c). The initial charge specific capacity was 156.1 mAh g^{-1} at 0.1 C, which was the same as that of the half cell, verifying the successful recovery of D-$LiFePO_4$. A high

https://doi.org/10.1021/acs.nanolett.3c01991
Nano Lett. XXXX, XXX, XXX−XXX

reversible capacity of 129.5 mAh g^{-1} was further achieved after 150 cycles at 1/3 C (virtual EV charge rate) with a high capacity retention of 86.3% (Figure 4d), showing the potential application of R-$LiFePO_4$ by targeted Li compensation.

Figure 4e,f shows cyclic voltammetry (CV) curves of D-$LiFePO_4$ and R-$LiFePO_4$ in the potential range of 2.7−4.2 V at 0.1 mV s^{-1}. D-$LiFePO_4$ displayed a weak oxidization peak at the first anodic scan process, in sharp contrast to the strong reduction peak at the cathodic scan process (Figure 4e). The low intensity of the oxidization peak in the first scan was caused by the low Li content of D-$LiFePO_4$. Such a peak showed similar intensity to the corresponding reduction peak in the following cycles, indicating that the Li deficiency in D-$LiFePO_4$ could be recovered by electrochemical Li filling. R-$LiFePO_4$ showed high intensity of the oxidization peak at the first scan, supporting the recovered Li loss after targeted chemical Li compensation (Figure 4f). Noted that the oxidation/reduction peaks were 3.54 and 3.32 V for both F-$LiFePO_4$ (Figures 4f and S9) and R-$LiFePO_4$ after the first cycle, and the reduction and oxidation peaks of R-$LiFePO_4$ were highly overlapped for different cycles, verifying the stable materials structure after regeneration.[39] Electrochemical impedance spectra (EIS) have been carried out for D-$LiFePO_4$ and R-$LiFePO_4$. The semicircle in the high-frequency region of the Nyquist plot represents the charge transfer resistance, and the slant rectilinear tail in the low-frequency region is the Warburg impedance. Before the first cycle, R-$LiFePO_4$ showed a much lower value of 64.8 Ω for the charge transfer resistance in contrast to 173.8 Ω for D-$LiFePO_4$, and it delivered a similar value of 47.6 Ω after the first cycle, indicating its good stability. Thus, the targeted chemical Li compensation not only addresses the Li deficiency and reduces the charge transfer resistance, but it also realizes a robust structure for stable electrochemical cycling.

In summary, we revealed the Li deficiency and stable framework of D-$LiFePO_4$ via a systematic materials structure investigation. The robust olivine phase of phosphate materials allows $LiFePO_4$ to endure more than 3000 cycles in batteries for EVs with a well-maintained crystal structure and only partial active Li loss. The Li loss during battery cycling caused the Li deficiency with the overall chemical formula of $Li_{1-x}FePO_4$, and phase separation featured olivine $FePO_4$ nanodomains (5−10 nm) embedded into the $LiFePO_4$ matrix. After one-pot chemical solution treatment, active Li was filled into the Li defect positions of the olivine phase, and the original electrochemical performance was recovered. Our study showed a paradigm of successful battery cathode materials regeneration based on the refinement of the degraded structure and composition, showing the potential low cost and high efficiency in comparison to the traditional metallurgy methods and thus demonstrating a promising future.

■ ASSOCIATED CONTENT

Supporting Information

The Supporting Information is available free of charge at https://pubs.acs.org/doi/10.1021/acs.nanolett.3c01991.

Experimental details and additional characterizations (PDF)

■ AUTHOR INFORMATION

Corresponding Author

Yongming Sun − *Wuhan National Laboratory for Optoelectronics, Huazhong University of Science and Technology, Wuhan 430074, China;* orcid.org/0000-0001-8528-525X; Email: yongmingsun@hust.edu.cn

Authors

Wenyu Wang − *Wuhan National Laboratory for Optoelectronics, Huazhong University of Science and Technology, Wuhan 430074, China*

Rui Wang − *School of Advanced Materials, Peking University, Shenzhen Graduate School, Shenzhen 518055, China*

Renming Zhan − *Wuhan National Laboratory for Optoelectronics, Huazhong University of Science and Technology, Wuhan 430074, China*

Junmou Du − *Wuhan National Laboratory for Optoelectronics, Huazhong University of Science and Technology, Wuhan 430074, China; Deepal Automobile Technology Co., Ltd., Chongqing 401120, China*

Zihe Chen − *Wuhan National Laboratory for Optoelectronics, Huazhong University of Science and Technology, Wuhan 430074, China*

Ruikang Feng − *Wuhan National Laboratory for Optoelectronics, Huazhong University of Science and Technology, Wuhan 430074, China*

Yuchen Tan − *Wuhan National Laboratory for Optoelectronics, Huazhong University of Science and Technology, Wuhan 430074, China*

Yang Hu − *Wuhan National Laboratory for Optoelectronics, Huazhong University of Science and Technology, Wuhan 430074, China*

Yangtao Ou − *Wuhan National Laboratory for Optoelectronics, Huazhong University of Science and Technology, Wuhan 430074, China*

Yifei Yuan − *College of Chemistry and Materials Engineering, Wenzhou University, Wenzhou 325035, China;* orcid.org/0000-0002-2360-8794

Cheng Li − *Neutron Scattering Division, Oak Ridge National Laboratory (ORNL), Oak Ridge, Tennessee 37831-6473, United States;* orcid.org/0000-0002-6546-6413

Yinguo Xiao − *School of Advanced Materials, Peking University, Shenzhen Graduate School, Shenzhen 518055, China;* orcid.org/0000-0001-9306-908X

Complete contact information is available at: https://pubs.acs.org/10.1021/acs.nanolett.3c01991

Notes

The authors declare no competing financial interest.

■ ACKNOWLEDGMENTS

This work is financially supported by the Natural Science Foundation of China (Grant No. 52072137, No. 52272207, and No. 52072888) and Innovation Fund of Wuhan National Laboratory for Optoelectronics of Huazhong University of Science and Technology. The authors would like to thank the Analytical and Testing Center of Huazhong University of Science and Technology. A portion of this research used resources at the Spallation Neutron Source, a DOE Office of Science User Facility operated by the Oak Ridge National Laboratory.

REFERENCES

(1) International Energy Agency. *Global EV Outlook 2023*; International Energy Agency, 2023. https://iea.blob.core.windows.net/assets/dacf14d2-eabc-498a-8263-9f97fd5dc327/GEVO2023.pdf (accessed 2023-03-30).

(2) Zhang, X.; Li, L.; Fan, E.; Xue, Q.; Bian, Y.; Wu, F.; Chen, R. Toward sustainable and systematic recycling of spent rechargeable batteries. *Chem. Soc. Rev.* **2018**, *47* (19), 7239−7302.

(3) Lv, W.; Wang, Z.; Cao, H.; Sun, Y.; Zhang, Y.; Sun, Z. A Critical Review and Analysis on the Recycling of Spent Lithium-Ion Batteries. *ACS Sustain. Chem. Eng.* **2018**, *6* (2), 1504−1521.

(4) Wu, X.; Ma, J.; Wang, J.; Zhang, X.; Zhou, G.; Liang, Z. Progress, Key Issues, and Future Prospects for Li-Ion Battery Recycling. *Glob. Chall.* **2022**, *6*, 2200067.

(5) Ciez, R. E.; Whitacre, J. F. Examining different recycling processes for lithium-ion batteries. *Nat. Sustain.* **2019**, *2* (2), 148−156.

(6) Aravindan, V.; Jayaraman, S.; Tedjar, F.; Madhavi, S. From Electrodes to Electrodes: Building High-Performance Li-Ion Capacitors and Batteries from Spent Lithium-Ion Battery Carbonaceous Materials. *ChemElectroChem.* **2019**, *6* (5), 1407−1412.

(7) Velázquez-Martínez, O.; Valio, J.; Santasalo-Aarnio, A.; Reuter, M.; Serna-Guerrero, R. A Critical Review of Lithium-Ion Battery Recycling Processes from a Circular Economy Perspective. *Batteries* **2019**, *5* (4), 68.

(8) Yang, L.; Feng, Y.; Wang, C.; Fang, D.; Yi, G.; Gao, Z.; Shao, P.; Liu, C.; Luo, X.; Luo, S. Closed-loop regeneration of battery-grade $FePO_4$ from lithium extraction slag of spent Li-ion batteries via phosphoric acid mixture selective leaching. *Chem. Eng. J.* **2022**, *431*, 133232.

(9) Song, Y.; Xie, B.; Song, S.; Lei, S.; Sun, W.; Xu, R.; Yang, Y. Regeneration of $LiFePO_4$ from spent lithium-ion batteries via a facile process featuring acid leaching and hydrothermal synthesis. *Green Chem.* **2021**, *23* (11), 3963−3971.

(10) Fan, E.; Li, L.; Wang, Z.; Lin, J.; Huang, Y.; Yao, Y.; Chen, R.; Wu, F. Sustainable Recycling Technology for Li-Ion Batteries and Beyond: Challenges and Future Prospects. *Chem. Rev.* **2020**, *120* (14), 7020−7063.

(11) Chen, X.; Cao, L.; Kang, D.; Li, J.; Zhou, T.; Ma, H. Recovery of valuable metals from mixed types of spent lithium ion batteries. Part II: Selective extraction of lithium. *Waste Manage.* **2018**, *80*, 198−210.

(12) Jie, Y.; Yang, S.; Li, Y.; Hu, F.; Zhao, D.; Chang, D.; Lai, Y.; Chen, Y. Waste Organic Compounds Thermal Treatment and Valuable Cathode Materials Recovery from Spent $LiFePO_4$ Batteries by Vacuum Pyrolysis. *ACS Sustain. Chem. Eng.* **2020**, *8* (51), 19084−19095.

(13) Liang, Q.; Yue, H.; Wang, S.; Yang, S.; Lam, K.-h.; Hou, X. Recycling and crystal regeneration of commercial used $LiFePO_4$ cathode materials. *Electrochim. Acta* **2020**, *330*, 135323.

(14) Xu, P.; Dai, Q.; Gao, H.; Liu, H.; Zhang, M.; Li, M.; Chen, Y.; An, K.; Meng, Y. S.; Liu, P.; Li, Y.; Spangenberger, J. S.; Gaines, L.; Lu, J.; Chen, Z. Efficient Direct Recycling of Lithium-Ion Battery Cathodes by Targeted Healing. *Joule* **2020**, *4* (12), 2609−2626.

(15) Shi, Y.; Chen, G.; Liu, F.; Yue, X.; Chen, Z. Resolving the Compositional and Structural Defects of Degraded $LiNi_xCo_yMn_zO_2$ Particles to Directly Regenerate High-Performance Lithium-Ion Battery Cathodes. *ACS Energy Lett.* **2018**, *3* (7), 1683−1692.

(16) Wang, T.; Luo, H.; Bai, Y.; Li, J.; Belharouak, I.; Dai, S. Direct Recycling of Spent NCM Cathodes through Ionothermal Lithiation. *Adv. Energy Mater.* **2020**, *10* (30), 2001204.

(17) Wu, C.; Hu, J.; Ye, L.; Su, Z.; Fang, X.; Zhu, X.; Zhuang, L.; Ai, X.; Yang, H.; Qian, J. Direct Regeneration of Spent Li-Ion Battery Cathodes via Chemical Relithiation Reaction. *ACS Sustain. Chem. Eng.* **2021**, *9* (48), 16384−16393.

(18) Wang, J.; Ma, J.; Jia, K.; Liang, Z.; Ji, G.; Zhao, Y.; Li, B.; Zhou, G.; Cheng, H.-M. Efficient Extraction of Lithium from Anode for Direct Regeneration of Cathode Materials of Spent Li-Ion Batteries. *ACS Energy Lett.* **2022**, *7* (8), 2816−2824.

(19) Du, M.; Guo, J.-Z.; Zheng, S.-H.; Liu, Y.; Yang, J.-L.; Zhang, K.-Y.; Gu, Z.-Y.; Wang, X.-T.; Wu, X.-L. Direct reuse of $LiFePO_4$ cathode materials from spent lithium-ion batteries: Extracting Li from brine. *Chin. Chem. Lett.* **2023**, *34* (6), 107706.

(20) Du, K.-D.; Meng, Y.-F.; Zhao, X.-X.; Wang, X.-T.; Luo, X.-X.; Zhang, W.; Wu, X.-L. A unique co-recovery strategy of cathode and anode from spent $LiFePO_4$ battery. *Sci. Chin. Mater.* **2022**, *65* (3), 637−645.

(21) Grey, C. P.; Tarascon, J. M. Sustainability and in situ monitoring in battery development. *Nat. Mater.* **2017**, *16* (1), 45−56.

(22) Fan, M.; Meng, Q.; Chang, X.; Gu, C.-F.; Meng, X.-H.; Yin, Y.-X.; Li, H.; Wan, L.-J.; Guo, Y.-G. In Situ Electrochemical Regeneration of Degraded $LiFePO_4$ Electrode with Functionalized Prelithiation Separator. *Adv. Energy Mater.* **2022**, *12* (18), 2103630.

(23) Wang, T.; Yu, X.; Fan, M.; Meng, Q.; Xiao, Y.; Yin, Y.-X.; Li, H.; Guo, Y.-G. Direct regeneration of spent $LiFePO_4$ via a graphite prelithiation strategy. *Chem. Commun.* **2020**, *56* (2), 245−248.

(24) Hess, M.; Sasaki, T.; Villevieille, C.; Novák, P. Combined operando X-ray diffraction-electrochemical impedance spectroscopy detecting solid solution reactions of $LiFePO_4$ in batteries. *Nat. Commun.* **2015**, *6* (1), 8169.

(25) Liu, H.; Strobridge, F. C.; Borkiewicz, O. J.; Wiaderek, K. M.; Chapman, K. W.; Chupas, P. J.; Grey, C. P. Capturing metastable structures during high-rate cycling of $LiFePO_4$ nanoparticle electrodes. *Science* **2014**, *344* (6191), 1252817.

(26) Jia, K.; Ma, J.; Wang, J.; Liang, Z.; Ji, G.; Piao, Z.; Gao, R.; Zhu, Y.; Zhuang, Z.; Zhou, G.; Cheng, H.-M. Long-Life Regenerated $LiFePO_4$ from Spent Cathode by Elevating the d-Band Center of Fe. *Adv. Mater.* **2023**, *35*, 2208034.

(27) Hu, J.; Huang, W.; Yang, L.; Pan, F. Structure and performance of the LiFePO 4 cathode material: from the bulk to the surface. *Nanoscale* **2020**, *12* (28), 15036−15044.

(28) Yuan, L.-X.; Wang, Z.-H.; Zhang, W.-X.; Hu, X.-L.; Chen, J.-T.; Huang, Y.-H.; Goodenough, J. B. Development and challenges of $LiFePO_4$ cathode material for lithium-ion batteries. *Energy Environ. Sci.* **2011**, *4* (2), 269−284.

(29) Tarascon, J. M.; Armand, M. Issues and challenges facing rechargeable lithium batteries. *Nature* **2001**, *414* (6861), 359−367.

(30) Hu, J.; Huang, W.; Yang, L.; Pan, F. Structure and performance of the $LiFePO_4$ cathode material: from the bulk to the surface. *Nanoscale* **2020**, *12* (28), 15036−15044.

(31) Padhi, A. K.; Nanjundaswamy, K. S.; Masquelier, C.; Okada, S.; Goodenough, J. B. Effect of Structure on the Fe^{3+}/Fe^{2+} Redox Couple in Iron Phosphates. *J. Electrochem. Soc.* **1997**, *144* (5), 1609−1613.

(32) Li, X.; Jiang, F.; Qu, K.; Wang, Y.; Pan, Y.; Wang, M.; Liu, Y.; Xu, H.; Chen, J.; Huang, Y.; Zheng, J.; Gao, P.; Chen, M.; Li, J.; Peng, Y.; Mitlin, D. First Atomic-Scale Insight into Degradation in Lithium Iron Phosphate Cathodes by Transmission Electron Microscopy. *J. Phys. Chem. Lett.* **2020**, *11* (12), 4608−4617.

(33) Cui, B.; Liu, C.; Zhang, J.; Lu, J.; Liu, S.; Chen, F.; Zhou, W.; Qian, G.; Wang, Z.; Deng, Y.; Chen, Y.; Hu, W. Waste to wealth: Defect-rich Ni-incorporated spent $LiFePO_4$ for efficient oxygen evolution reaction. *Sci. China Mater.* **2021**, *64*, 2710−2718.

(34) Ji, G.; Wang, J.; Liang, Z.; Jia, K.; Ma, J.; Zhuang, Z.; Zhou, G.; Cheng, H. Direct regeneration of degraded lithium-ion battery cathodes with a multifunctional organic lithium salt. *Nat. Commun.* **2023**, *14*, 584.

(35) Dedryvère, R.; Maccario, M.; Croguennec, L.; Le Cras, F.; Delmas, C.; Gonbeau, D. X-Ray Photoelectron Spectroscopy Investigations of Carbon-Coated $LixFePO_4$ Materials. *Chem. Mater.* **2008**, *20* (22), 7164−7170.

(36) Laffont, L.; Delacourt, C.; Gibot, P.; Wu, M. Y.; Kooyman, P.; Masquelier, C.; Tarascon, J. M. Study of the $LiFePO_4/FePO_4$ Two-Phase System by High-Resolution Electron Energy Loss Spectroscopy. *Chem. Mater.* **2006**, *18* (23), 5520−5529.

(37) Liu, X.; Liu, T.; Wang, R.; Cai, Z.; Wang, W.; Yuan, Y.; Shahbazian-Yassar, R.; Li, X.; Wang, S.; Hu, E.; Yang, X.-Q.; Xiao, Y.; Amine, K.; Lu, J.; Sun, Y. Prelithiated Li-Enriched Gradient

https://doi.org/10.1021/acs.nanolett.3c01991
Nano Lett. XXXX, XXX, XXX−XXX

Interphase toward Practical High-Energy NMC-Silicon Full Cell. *ACS Energy Lett.* **2021**, *6* (2), 320−328.
(38) Liu, X.; Tan, Y.; Wang, W.; Li, C.; Seh, Z. W.; Wang, L.; Sun, Y. Conformal Prelithiation Nanoshell on LiCoO2 Enabling High-Energy Lithium-Ion Batteries. *Nano Lett.* **2020**, *20* (6), 4558−4565.
(39) Tao, R.; Li, F.; Lu, X.; Liu, F.; Xu, J.; Kong, D.; Zhang, C.; Tan, X.; Ma, S.; Shi, W.; Mo, R.; Lu, Y. High-Conductivity-Dispersibility Graphene Made by Catalytic Exfoliation of Graphite for Lithium-Ion Battery. *Adv. Funct. Mater.* **2021**, *31* (6), 2007630.

https://doi.org/10.1021/acs.nanolett.3c01991
Nano Lett. XXXX, XXX, XXX−XXX